JOURNAL OF MATERIALS SCIENCE 10 (1975) 1275–1284

Electron microscopy of microcracking about indentations in aluminium oxide and silicon carbide

B. J. HOCKEY, B. R. LAWN*
Institute for Materials Research, National Bureau of Standards, Washington, D.C., USA

Transmission electron microscopy is used to examine the nature of microcracking about small-scale indentations in two highly brittle solids, sapphire and carborundum. The observed crack geometry is discussed in terms of an earlier model of indentation fracture beneath a point force, in which both loading and unloading half-cycles contribute to the crack growth. The residual interfaces are generally found to exhibit moiré fringe contrast, and occasionally to contain dislocation networks. These observations are discussed in relation to spontaneous closure and healing mechanisms, and the associated "lattice mismatch" is estimated at about one part in a thousand. It is suggested that cleavage steps comprise the main source of obstruction to lattice restoration across the interfaces. Mechanical and thermal treatments of the indented specimens are found to influence the extent of the residual cracking. Some practical implications concerning the strength degradation of brittle solids are discussed.

1. Introduction

Indentation hardness testing is finding an increased usage in the scientific investigation of damage processes in highly brittle solids [1]. A suitably sharp indenter tip concentrates very high levels of stress, particularly in shear and hydrostatic compression, and thus induces irreversible deformation in conveniently localized regions of a test surface. In many brittle materials the mean contact pressure can be as much as a tenth of an elastic modulus [2], indicating that the intrinsic bond strength of the lattice itself must surely be exceeded in places. Despite a recent proliferation of indentation damage studies, the exact nature of such irreversible deformation processes in brittle solids remains something of a contentious issue.

One aspect of indentation damage which has been largely overlooked is that of indentation-induced cracking. In the general indentation field a component of tension, however small, is unavoidable [3], and there is a growing body of evidence suggesting that cracking may be more prevalent that one might have been led to believe from earlier studies. An understanding of indentation fracture is important for many practical as well as academic reasons (for a review see [4]): a pertinent example is strength degradation as a result of particle-surface contact, where individual damage events may be usefully simulated in a standard hardness testing device.

The chief object of this work is to report on observations of microcrack patterns about small-scale point indentations in aluminium oxide and silicon carbide, two highly brittle materials currently of great interest in ceramics engineering. The results represent part of a detailed study of residual crack interfaces using transmission electron microscopy. Our emphasis here is directed to geometrical features of the observed crack interfaces. The observed crack geometry is discussed in terms of an earlier proposal for crack growth beneath sharp indenters based on optical observations [3]. The study complements an analysis of diffraction contrast effects at large-scale remnant cone cracks in sphere-indented silicon, using X-ray topography [5].

*On study leave, from School of Physics, University of New South Wales, Kensington, N.S.W. 2033, Australia.

2. Preparation of indentation specimens for electron microscopy

The method of specimen preparation was similar to that previously described [6-8]. Single crystals of sapphire and α-silicon carbide were cut into slabs and polished, first mechanically and then chemically, to a thickness of about 100 μm. Indentations were made with either a Knoop or Vickers diamond pyramid at a load of 200 g on each test surface. An optical examination of the surfaces showed clear evidence of microcracking in most cases, especially about the Vickers indentations. The crystals were then thinned to a size suitable for 200 kV transmission electron microscopy by ion bombardment [7]. Most of the material removed was from the surface below the indentation, although a little ($\approx$ 1 μm) was removed from the top surface as well to eliminate any spurious damage incurred in specimen handling.

Most of the foils examined were prepared at room temperature. However, a few were subjected to prescribed thermal or mechanical treatments between the indentation and thinning stages, as described in [8]. About one-hundred indentations in sapphire, and about twenty-five in silicon carbide, were investigated in this way.

3. Electron microscopy of cracks

3.1. General crack morphology

Intense diffraction contrast was observed in the immediate vicinity of all impressions. At the edges of the impressions, the images of dislocations, and sometimes of twins as well, could be clearly resolved. An analysis of this deformation has been given in the case of sapphire in an earlier paper [7], and similar deformation patterns have recently been analysed in indented silicon [9, 10]. The diffraction spot pattern was maintained at all locations in the foils, although considerable broadening of the spots was evident in the most heavily deformed regions. No diffraction evidence was found for any crystallographic phase transformation resulting from the indentation process.

Cracking was observed about all Vickers impressions examined, and about most Knoop impressions. With the Vickers specimens, cracks were always observed to extend radially outward from the corners of the indentations, their plane oriented very nearly normal to the foil surfaces, as seen clearly in Fig. 1 (silicon carbide). In addition, cracks lying nearly parallel to the foil surfaces were often observed between the radial cracks, again as in Fig. 1, but the geometry and indeed the frequency of appearance of this type

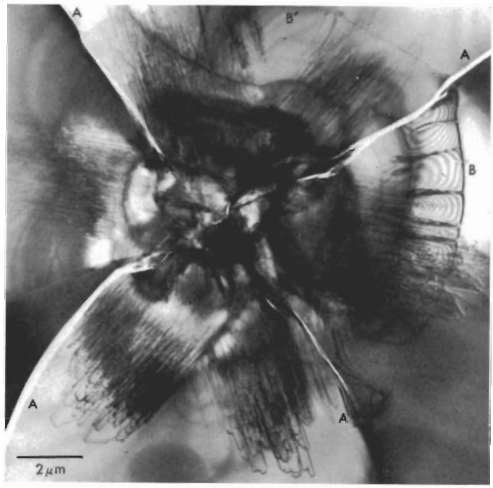

Figure 1 Transmission electron micrograph showing typical configuration of dislocations and cracks associated with a room temperature 200 g Vickers indentation on the (0001) plane of α-SiC (4H polytype structure). Two distinct crack configurations are evident: A, radially directed cracks extending from corners of pyramidal impression, and B, cracks lying parallel to foil either partially or fully encircling central deformation zone (see also Figs. 8 and 10).

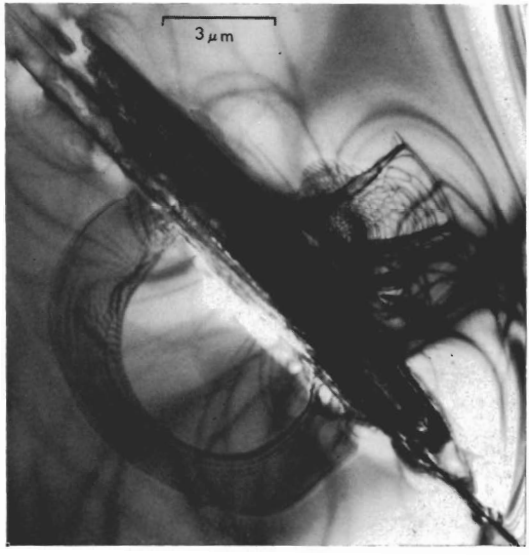

Figure 2 Transmission electron micrograph showing room temperature 200 g Knoop indentation on the $(10\bar{1}0)$ plane of Al_2O_3. Note crack remnants extending from sides of central deformation zone. Geometry of cracks depicted in Fig. 5.

of crack were sporadic. In the case of Knoop specimens, for example Fig. 2 (sapphire), the incidence of detectable radial cracking was considerably less than for Vickers specimens, but for the lateral type of cracking the incidence was almost the same.

These observations may be readily explained in terms of the scheme for crack growth beneath sharp indenters put forward by Lawn and Swain [3]. Basically, two distinct stages of crack formation are apparent. The first occurs on indenter *loading*; at some (low) threshold level of stress a crack initiates at the deformation zone immediately below the sharp point of the indenter and extends downward on a plane of symmetry containing the contact axis. Fig. 3 depicts schematically the shape of this crack, the so-called "median vent crack", in its well-developed

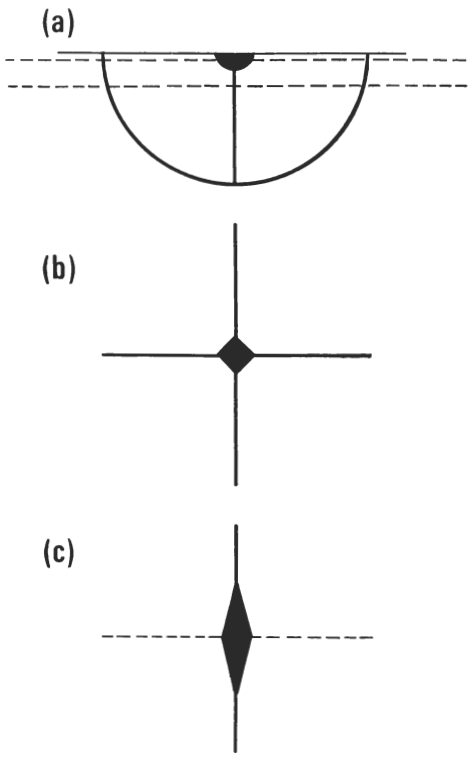

Figure 3 Schematic presentation of median vent cracks, formed during indenter *loading*. Cracks are indicated by full, heavy lines, central deformation zone by dark region. (a) Section view, for both Vickers and Knoop indenters; location of eventual thin foil indicated by dashed lines. (b) Plan view, for Vickers indenter; crack tends to extend well beyond central zone, along both diagonals. (c) Plan view, for Knoop indenter; crack tends to be obscured below central zone, and to grow only along major diagonal.

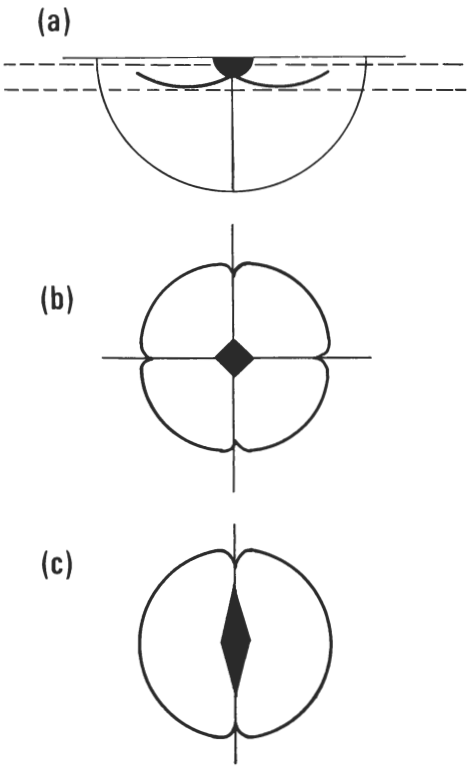

Figure 4 Schematic representation of lateral vent cracks, formed during indenter *unloading*. Cracks are indicated by full, heavy lines (preceding median vent cracks by full, light lines), central deformation zone indicated by dark region. (a) Section view, for both Vickers and Knoop indenters; location of eventual thin foil indicated by dashed lines. (b) Plan view, for Vickers indenter. (c) Plan view, for Knoop indenter. Note lateral vents tend to form as lobes between the median vents.

form. Fig. 3a indicates how the thinned foil samples the crack about the deformation zone. The median vents accordingly appear as ribbon-like segments along the lines of greatest stress concentration, as depicted in Fig. 3b for the Vickers and Fig. 3c for the Knoop specimens respectively. It is clear that the shape of the remnant crack will not be too sensitive to the exact location of the foil with respect to the original indented surface. The second stage of crack formation occurs on *unloading*; just prior to removal of the indenter new cracks initiate at the deformation zone and extend sideways into a shallow saucer-shaped configuration, modified to some extent by the presence of the median vents. This crack, the "lateral vent", is depicted in Fig. 4. In this case the location of the foil becomes a

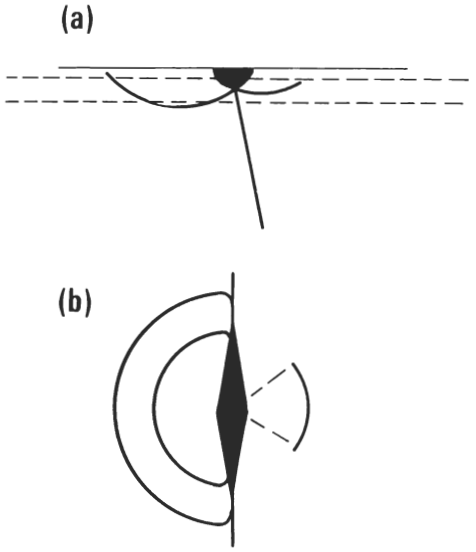

Figure 5 Effect of skew loading on crack pattern for Knoop indenter. Depicted to match loading conditions for the indentation illustrated in Fig. 2. (a) Section view. (b) Plan view.

critical factor; small changes in the relative amounts of material removed from the upper and lower surfaces of the indented crystal during thinning might result in the loss of a portion, if not all, of the lateral vent system. One further, very important consideration in connection with the geometry of remnant lateral vents is the axis of loading; in practice it is no easy matter to ensure near-perpendicularity between indenter axis and specimen surface, and preferred cracking on one side of the indentation tends to be the rule rather than the exception. In Fig. 5 we indicate how such asymmetry accounts for the apparently complex crack morphology seen in the electron micrograph of Fig. 2.*

3.2. Interfacial fringe and dislocation contrast

An examination of the diffraction contrast of the remnant cracks provides quantitative evidence for residual lattice mismatch across the interfaces. Essentially, the crack images are typified by fringe and dislocation networks. Figs. 6 and 7, showing median vents about Vickers indents in silicon carbide and sapphire respectively, and Figs. 8 and 9, showing lateral vents about a Vickers indent in silicon carbide and a Knoop

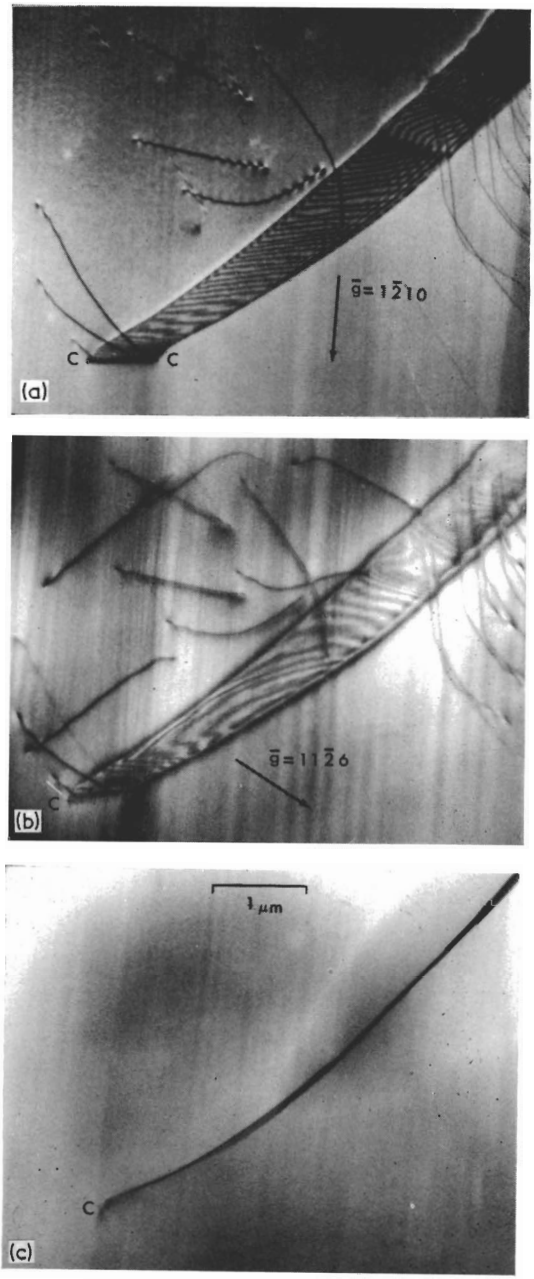

Figure 6 Median vent type crack associated with 200 g Vickers indentation on (0001) plane of α-SiC, seen under different diffracting conditions. Crack front indicated as CC. (a) and (b) satisfy Laue reflection conditions, diffraction vectors shown. (c) is view of crack obtained by tilting specimen, multiple reflections. Note change in mismatch fringe pattern in (a) and (b) with diffraction vector. Specimen indented at room temperature and annealed in air at 1200° C for four h prior to thinning.

*A distinct example of such asymmetry in crack pattern due to inclined loading of a Knoop indenter on a quartz surface may be seen in Fig. 7 of [3].

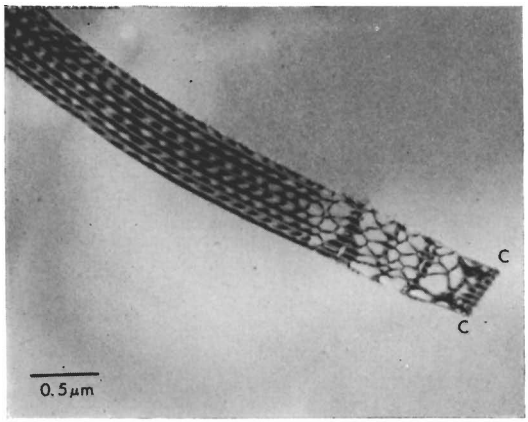

Figure 7 Portion of median vent crack associated with room temperature 200 g Vickers indentation on (0001) plane of Al_2O_3. Note complex fringe pattern over greater part of crack interface, with interfacial dislocation network near crack front CC. Multiple reflections operating.

indent in sapphire respectively, are examples. The patterns in all cases are largely characteristic of *mismatch contrast* [11, 12], generated by interference between slightly mismatched, simultaneously diffracting portions of crystal across the crack interfaces, although there is some indication of *thickness fringe* modulation where the interface is inclined to the foil surface (e.g. Fig. 7). This diagnosis was confirmed by observing the spacing of the fringes to remain invariant with voltage of the electron beam in the microscope (e.g. by lowering from 200 kV to 100 kV) [11].

Fringe patterns of the mismatch type associated with residual cavities or cracks may be categorized into either *displacement* or *moiré* systems [12]. The displacement system is generated when the opposing crystal portions are separated by a rigid-body displacement $\mathbf{c}(\mathbf{r})$, where $\mathbf{r}$ is a position vector contained within the interface and measured from the crack tip: if the diffraction vector (i.e. reciprocal vector defining orientation and spacing of lattice planes) in both crystallites is $\mathbf{g}$, the fringes are loci of

$$\mathbf{g} \cdot \mathbf{c} = N \qquad (1)$$

where N is the order of the fringe [12]. Thus one characteristic of the displacement fringe system is that the observed pattern should remain geometrically similar for all reflections. In Figs. 6 and 8, where the effects of systematically varying $\mathbf{g}$ are investigated, the geometry of the

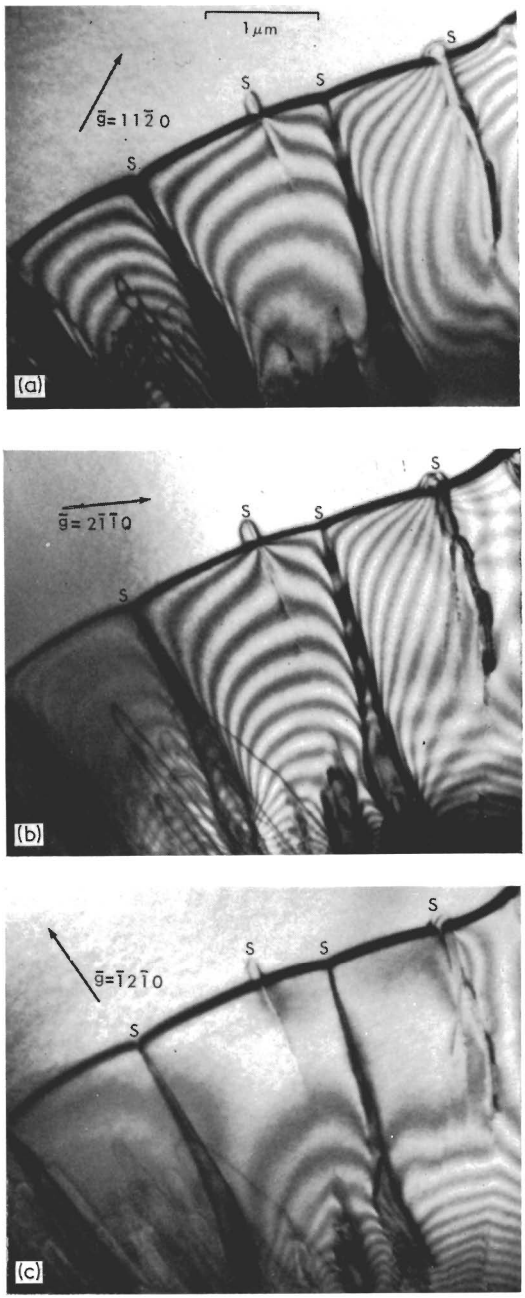

Figure 8 Enlargement of lateral vent segment B in Fig. 1, under different reflecting conditions. Note tendency for fringes to run nearly parallel to the crack front, with modification in patterns at steps, S, which terminate at crack front. Diffraction vectors indicated.

fringe pattern is seen to change markedly. Moreover, the reflections in Fig. 8 are such that we would have $\mathbf{g} \cdot \mathbf{c} \approx 0$ if the mutual crack-wall

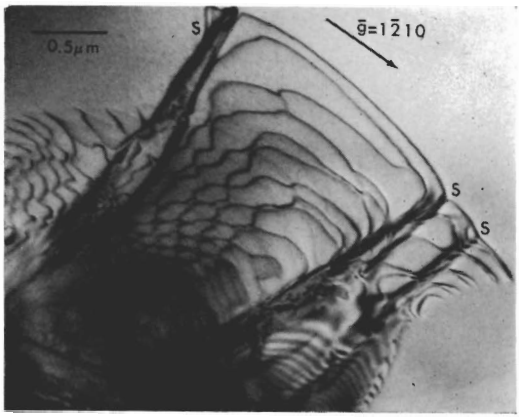

Figure 9 Enlargement of lateral vent at right in Fig. 2. Note interfacial dislocation network between steps, S, which terminate at crack front.

displacements were, as anticipated, to be closely normal to the plane of the interface (hence of the foil). We must generally conclude that the displacement fringe system can be of no more than secondary importance in the micrographs observed in this work.

The moiré fringe system, on the other hand, is generated when the overlapping crystal portions have a small mismatch in lattice periodicity such that there is a small difference in diffraction vector, $\delta\mathbf{g} = \mathbf{g}_1 - \mathbf{g}_2 \neq 0$. The fringes are then loci of [13, 14]

$$\delta\mathbf{g} \cdot \mathbf{r} = \text{const}. \qquad (2)$$

Then, since $\delta\mathbf{g}$ will generally vary with $\mathbf{g}$, we would expect such a pattern to be reflection-dependent, consistent with the observations of Figs. 6 and 8. This diagnosis in favour of the moiré system was also reached in the earlier X-ray analysis of remnant cone cracks in silicon [5]. In the event that the opposing crack walls are able to recontact and heal, interfacial relaxation of the mismatched crystal portions results in a dislocation network [8, 15]. Examples of spontaneous crack healing are seen in Figs. 7 (near-tip region) and 9.

It is of interest to determine the degree of mismatch needed to explain the network patterns seen in the micrographs. Characterizing the fringe system associated with the non-healed crack interfaces by the moiré vector (i.e. reciprocal vector defining orientation and spacing of fringe system) [13]

$$\mathbf{G} = \delta\mathbf{g} = \mathbf{g}_1 - \mathbf{g}_2, \qquad (3)$$

we distinguish between two basic moiré configurations: *parallel* moirés, in which $\mathbf{g}_1$ and $\mathbf{g}_2$ differ slightly in magnitude ($\mathbf{G}$ parallel to $\mathbf{g}$), and *rotation* moirés, in which $\mathbf{g}_1$ and $\mathbf{g}_2$ differ slightly in direction ($\mathbf{G}$ perpendicular to $\mathbf{g}$). In most cases examined here the system appeared to be predominantly of the second type; note in particular the comparative absence of fringe contrast in Fig. 8c, corresponding to $\mathbf{G}$ having a large component parallel to $\mathbf{g}$. Such a lattice-plane rotation is, in fact, consistent with a simple shear displacement field $\mathbf{u} = u_z(r)\hat{\mathbf{z}}$ ($\hat{\mathbf{z}}$ being a unit vector parallel to the crack front) for the crack walls at the interface (i.e. "mode III" field). Writing $d = |\mathbf{g}|^{-1}$ as the spacing of the lattice planes and $D = |\mathbf{G}|^{-1}$ as the spacing of the moiré fringes, we obtain

$$\frac{D}{d} \approx \frac{1}{\epsilon} \quad \text{(rotation)} \qquad (4)$$

with ϵ the angular misorientation of the diffracting planes. Typically, we have $d_{11\bar{2}0} \approx 0.15$ nm (α-SiC), $D \approx 0.1$ μm (Fig. 8), from which we compute a "lattice mismatch" $d/D \approx 1 \times 10^{-3}$; this corresponds to a mutual lattice-plane misorientation $\epsilon \approx u_z(r)/r \approx 1 \times 10^{-3}$ rad.

Our treatment here is necessarily oversimplistic: a more accurate account of fringe pattern details would require a rigorous diffraction contrast analysis, taking into account such complications as inclinations of the interface to the foil surface [14], superposition of components $u_y(r)\hat{\mathbf{y}}$ and $u_x(r)\hat{\mathbf{x}}$ ($\hat{\mathbf{y}}$ and $\hat{\mathbf{x}}$ being unit vectors parallel to crack normal and crack direction respectively) onto the residual displacement field (i.e. adding "modes I and II" to "mode III"), etc., in the general reflection situation.

3.3. Other interfacial features in the crack images

Some other contrast features were evident at the residual crack interfaces. The crack front itself usually showed up by enhanced diffraction contrast, implying residual crack-tip strain due to incomplete closure of the interface. This residual-strain effect was more evident in some cases (e.g. Fig. 8) than others (e.g. Fig. 7); in general, those interfaces indicating some tendency to healing showed the least crack-tip contrast. In addition, the contrast visibility increased in intensity from zero as the $\mathbf{g}$ vector was rotated away from alignment with the crack front, in accordance with a state of plane strain

at the tip: a particularly clear example of this contrast variation is shown in Fig. 10.

The existence of a residual crack opening points to the operation of some closure-prevention mechanism. While there was ample indication of dislocation generation about the central, grossly deformed regions of the indentations, in no case was there found any evidence for dislocation activity in association with crack growth, thus ruling out plastic flow as a significant factor.* The present observations merely reinforce similar conclusions previously drawn concerning the reversibility of fracture in highly brittle solids [5, 8, 15]. Closure resistance may be identified with purely mechanical obstruction, predominantly from cleavage steps at the fracture surfaces [5]. These are seen clearly in many of the micrographs, notably in Figs. 8 and 9. A close study of the mechanics of formation of such steps [16] indicates a process in which crack segments propagating on closely adjacent planes first overlap and subsequently link up tip-to-plane to effect separation. Segmentation of an initially planar crack into an array of partial fronts occurs when a "twist-mode" disturbance is suddenly encountered in the crack propagation field [17]. Fig. 11 depicts the phenomenon schematically, and illustrates via the fringe pattern in the accompanying micrograph the significant influence the stepped regions have on the residual crack opening. The smallest of lateral displacements across the crack interface, corresponding to the lattice mismatch of order one part in a thousand typified by the fringe spacings, could be quite sufficient to prevent the opposing walls from keying together in perfect registry upon removal of the indenter load. Moreover, these same lateral displacements would account for a predominance of a mode III type configuration in the moiré system.

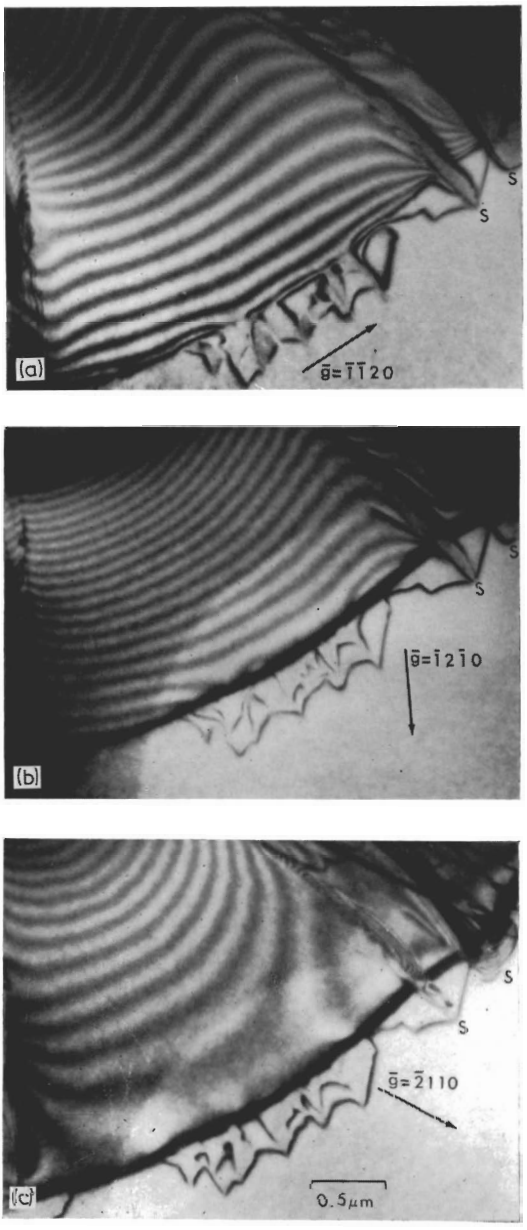

Figure 10 Enlargement of lateral vent segment B′ in Fig. 1, under different reflecting conditions. Note disappearance of crack-tip contrast for g parallel to front. Note also presence of features exhibiting dislocation-like contrast ahead of residual crack front. Step-contrast, S, indicates extent to which crack front must once have propagated.

One further detail which was observed in isolated cases was the trace of a slightly retracted crack front. This is especially noticeable in Fig. 10, where protuberant cleavage-step damage beyond the residual interfacial opening gives some indication as to how far the crack front must once have extended. The exact source of this detail is not clear, but its contrast parallels that of dislocations and thus probably arises from residual displacements on the atomic scale.

3.4. Cracks subjected to special treatments

Some of the indented sapphire specimens were subjected to a mechanical shock treatment prior to thinning. This was done simply by delivering

*The healing dislocations do not, of course, form via a glide process, but rather as a direct consequence of crack closure: they could, therefore, hardly contribute to a residual crack opening.

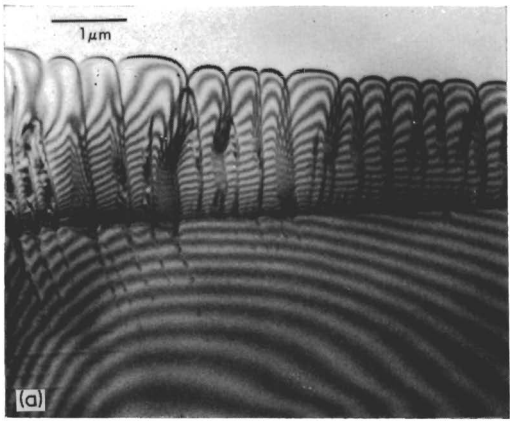

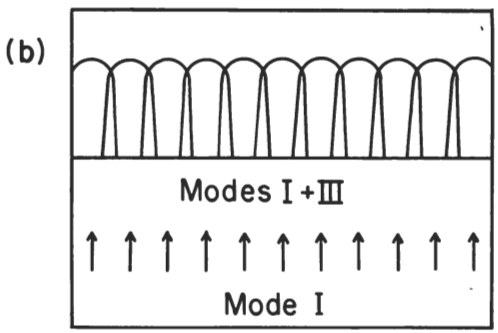

Figure 11 (a) Portion of remnant crack front associated with room temperature 200 g Vickers indentation on (0001) α-SiC. (b) Schematic representation, showing how crack breaks up into partial fronts upon encountering some shear disturbance. Arrows indicate direction of propagation of main crack.

a small impulse, insufficient to rupture the specimen, to the surface opposite to that containing the indentations. The chief result of this treatment was to re-propagate the existing *median* vent cracks (the lateral vents suffering effectively zero tension in the flexural impulse), to anything up to an order of magnitude increase in length, rather than to change the nature of the patterns. These extended crack portions also showed some tendency to partial spontaneous healing [8].

Other specimens were given an anneal treatment. In this case diffusion and sintering processes led to a marked enhancement in the healing [8]. Fig. 12 shows a remnant interface at which the delineation between restored and non-restored interfacial regions is distinct. Elongated "pipes" are seen to form along lines of greatest residual mismatch, namely along network dislocations, but these tend ultimately to break up into small polyhedral voids in the regions of more prolonged sintering away from the open interface.

4. Discussion

The observations described here provide useful semi-quantitative information on the geometry of residual cracks about micro-indentations. It should be emphasized, however, that this information relates only to the history of the propagation, and not the *initiation*, of the cracks. That is to say, nothing in the electron micrographs revealed any indication as to how the cracks originally nucleated and formed. It is known from earlier section-and-etch examinations [3] that median- and lateral-vent initiation are both tied up intimately with events within the gross deformation zone immediately surrounding the indenter; unfortunately, this is the region of lost resolution and diffraction-pattern blurring (Section 3.1), and, while it is clear that the theoretical strength limits of the lattice are undoubtedly approached (at least in the most brittle of solids), the nature of indentation-induced deformation remains obscure [9, 10, 18, 19]. This is one aspect of the indentation problem which calls for a good deal more attention.

Although we have given explicit attention here to only sapphire and α-silicon carbide, the crack patterns described appear to be quite typical of

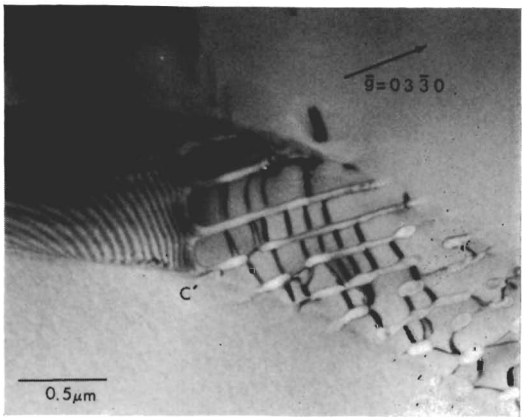

Figure 12 Median vent crack remnant associated with room temperature 200 g Vickers indentation on (0001) Al_2O_3. Indented specimen annealed at 1200 C in air for 8 h prior to thinning. Annealing results in recession of crack front to C′C′, with healed (sintered) region characterized by interfacial dislccations and voids, and unhealed (open) region characterized by mismatch fringe contrast.

highly brittle solids in general. In particular, the vent-crack systems show the same broad geometrical features evident in such structurally diverse materials as monocrystalline silicon and amorphous silicates [3, 20], thus emphasizing the dominant role of the indentation stress field in determining the fracture paths. Nevertheless, preferred cleavage tendencies do usually have some effect on indentation-cracking geometry [4, 21], and crystallographic tendencies were indeed noted in the present observations. In this respect the materials studied in the present work provide an interesting contrast in that α-silicon carbide has a distinct tendency to basal cleavage while sapphire does not, the reason being that although (0001) may represent the plane intersecting the least number of bonds in the hexagonal structure a relatively large component of polarity in the bonding in the case of sapphire renders this plane unfavourable on the grounds of electrostatic attraction effects [22]. One would, therefore, anticipate a greater incidence of lateral venting nearly parallel to (0001) foils in the former material; this trend was in fact apparent in the micrographs (note extensive crack plane in Figs. 8 and 10, not generally seen in sapphire). This raises the question of *anisotropy* in the microfracture, a factor which has already been recognized as one of vital importance in the interpretation of deformation processes in hardness testing [23]. One striking manifestation of anisotropy in a (cumulative) indentation chipping process occurs in the abrasion of diamond; by changing the abrasion direction on a given surface the wear rate may alter by as much as three orders of magnitude [24]. Anisotropy is, therefore, a second topic which warrants further consideration in relation to indentation fracture.

The present results also bear on the process of crack healing, and on the agencies which tend to obstruct it. In those special instances where spontaneous healing was observed, evidence of cleavage steps and "debris" at the interface was conspicuously absent [15]. (It is possible, of course, that the very act of thinning the foil removes, at least partially, some of these obstructions.) Here again the two materials examined showed contrasting behaviour, for the only sighting of a spontaneously healed area in silicon carbide was that shown in Fig. 10. The nature of the bonding thus appears to manifest itself in the mechanics of the closure as well as of the opening of the cracks; the explanation is once more to be sought in the long-range electrostatic attractive forces that tend to develop across fracture interfaces in ionic structures [25, 26]. The second type of healing reported here, that arising from mass transport at elevated temperatures, occurs in both materials. On the other hand, while indentation-induced cracks can be made to heal, so can they be made to extend still further, as in the event of mechanical shock. The existence of residual cracks of this sort has obvious implications in the strength of structural ceramics: an incompletely restored lattice across any separation interface represents a potential source of weakness in the material. A more detailed investigation into electron-microscopic images of fracture interfaces is accordingly under way, and will be reported at a later date [27]. For the present, it is sufficient to point out that the strengths of brittle materials can be seriously degraded by the most minute of contact events, and that this degradation may vary according to subsequent mechanical and thermal history.

Acknowledgements

The authors are indebted to S. M. Wiederhorn and M. V. Swain for valuable discussions on the work. They also acknowledge the sponsorship by the Office of Naval Research under Contract No. NR-032-535.

References

1. J. H. WESTBROOK and H. CONRAD (eds.), "The Science of Hardness Testing and its Research Applications", Symposium Proceedings (American Society for Metals, Metals Park, Ohio, 1973).
2. A. KELLY, "Strong Solids" (Clarendon Press, Oxford, 1966) Ch 1.
3. B. R. LAWN and M. V. SWAIN, *J. Mater. Sci.* **10** (1975) 113.
4. B. R. LAWN and T. R. WILSHAW, *J. Mater. Sci.* **10** (1975) 1049.
5. J. S. WILLIAMS, B. R. LAWN and M. V. SWAIN, *Phys. Stat. Sol.* (*a*) **2** (1970) 7.
6. B. J. HOCKEY, in "The Science of Hardness Testing and its Research Applications", edited by J. H. Westbrook and H. Conrad (American Society for Metals, Metals Park, Ohio, 1973) Ch. 30.
7. B. J. HOCKEY, *J. Amer. Ceram. Soc.* **54** (1971) 223.
8. S. M. WIEDERHORN, B. J. HOCKEY and D. E. ROBERTS, *Phil. Mag.* **28** (1973) 783.
9. V. G. EREMENKO and V. I. NIKITENKO, *Phys. Stat. Sol.* (*a*) **14** (1972) 317.
10. M. J. HILL and D. J. ROWCLIFFE, *J. Mater. Sci.* **9** (1974) 1569.
11. P. B. HIRSCH, A. HOWIE, R. B. NICHOLSON,

D. W. PASHLEY and M. J. WHELAN, "Electron Microscopy of Thin Crystals" (Plenum, New York, 1965).
12. U. BONSE, M. HART and G. H. SCHWUTTKE, *Phys. Stat. Sol.* **33** (1969) 361.
13. R. GEVERS, *Phil. Mag.* **7** (1962) 1681.
14. R. GEVERS, J. VAN LANDUYT and S. AMELINCKX, *Phys. Stat. Sol.* **18** (1966) 325.
15. B. R. LAWN and T. R. WILSHAW, "Fracture of Brittle Solids" (Cambridge University Press, Cambridge, 1975) Ch. 2.
16. M. V. SWAIN, B. R. LAWN and S. J. BURNS, *J. Mater. Sci.* **9** (1974) 175.
17. E. SOMMER, *Eng. Fract. Mech.* **1** (1969) 539.
18. I. V. GRIDNEVA, YU V. MILMAN and V. I. TREFILOV, *Phys. Stat. Sol.* (*a*) **14** (1972) 177.
19. F. M. ERNSBERGER, *Ann. Rev. Mat. Sci.* **2** (1972) 529.
20. D. J. ROWCLIFFE, unpublished work.
21. B. R. LAWN, *J. Appl. Phys.* **39** (1968) 4828.
22. G. A. WOLFF and J. D. BRODER, *Acta Cryst.* **12** (1959) 313.
23. C. A. BROOKES, J. B. O'NEILL and B. A. W. REDFERN, *Proc. Roy. Soc. Lond.* **A322** (1971) 73.
24. E. M. WILKS and J. WILKS, *Phil. Mag.* **4** (1959) 158.
25. P. J. BRYANT, L. H. TAYLOR and P. L. GUTSHALL, "Transactions of the Tenth National Vacuum Symposium" (Macmillan, New York, 1963) p. 21.
26. J. A. RYAN and J. J. GROSSMAN, *Science J.* **4** (1968) 41.
27. B. J. HOCKEY, to be published.

Received 1 January and accepted 17 January 1975.